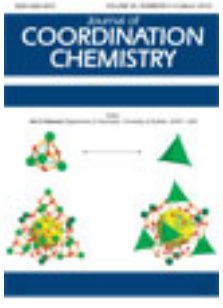

Journal of Coordination Chemistry
Publication details, including instructions for authors and subscription information:
http://www.tandfonline.com/loi/gcoo20

New supramolecular ferrocenyl amides: synthesis, characterization, and preliminary DNA-binding studies

Fatima Javed [a], Ataf Ali Altaf [a], Amin Badshah [a], Muhammad Nawaz Tahir [b], Muhammad Siddiq [a], Zia-Ur-Rehman [a], Afzal Shah [a], Shafiq Ullah [a] & Bhajan Lal [a]

[a] Department of Chemistry, Quaid-i-Azam University, Islamabad-45320, Pakistan

[b] Department of Physics, University of Sirgodah, Sirgodah, Pakistan

Published online: 27 Feb 2012.

To cite this article: Fatima Javed, Ataf Ali Altaf, Amin Badshah, Muhammad Nawaz Tahir, Muhammad Siddiq, Zia-Ur-Rehman, Afzal Shah, Shafiq Ullah & Bhajan Lal (2012) New supramolecular ferrocenyl amides: synthesis, characterization, and preliminary DNA-binding studies, Journal of Coordination Chemistry, 65:6, 969-979, DOI: 10.1080/00958972.2012.664769

To link to this article: http://dx.doi.org/10.1080/00958972.2012.664769

Journal of Coordination Chemistry
Vol. 65, No. 6, 20 March 2012, 969–979

New supramolecular ferrocenyl amides: synthesis, characterization, and preliminary DNA-binding studies

FATIMA JAVED†§, ATAF ALI ALTAF†§, AMIN BADSHAH*†, MUHAMMAD NAWAZ TAHIR‡, MUHAMMAD SIDDIQ†, ZIA-UR-REHMAN†, AFZAL SHAH†, SHAFIQ ULLAH† and BHAJAN LAL†

†Department of Chemistry, Quaid-i-Azam University, Islamabad-45320, Pakistan
‡Department of Physics, University of Sirgodah, Sirgodah, Pakistan

(*Received 23 November 2011; in final form 9 January 2012*)

Three ferrocenyl amides have been synthesized and characterized by analytical techniques. Based on single-crystal X-ray analysis, a supramolecular structure was attributed to **1** owing to the presence of intermolecular non-covalent interactions. UV-Visible spectroscopy, viscometry, and dynamic laser light scattering was used to assess the mode of interaction and binding of these complexes with DNA, which varied in the sequence **1** > **2** > **3**. The binding is presumably due to the ability of these complexes to form secondary non-covalent interactions with DNA bases. Complex-DNA adduct formation depends on the nature of *R* of the amide.

Keywords: Ferrocenyl amide; DNA-binding; Non-covalent interaction

1. Introduction

The main cause of diseases such as cancer, diabetes, and hemophilia, is related to over or under production of proteins or mutated proteins. As DNA is the genetic material that codes for proteins, drug interactions with DNA which can affect the replication processes are potential treatments for such diseases. Two broad classes of non-covalent DNA-binding agents have been identified, intercalators and groove binders. Intercalators bind by inserting a planar aromatic chromophore between adjacent DNA base pairs, whereas groove binders fit into the grooves of DNA causing little perturbation of the DNA structure. Small molecules have been extensively used as therapeutic agents in biotechnology due to their cost effective synthesis and comparatively efficient cellular delivery [1]. Many aspects of the rich literature concerning drug binding to DNA have been reviewed in recent articles, symposia, and books [2–4].

Metal-based compounds as biological probes represent one of the most successful applications of bioinorganic chemistry. DNA-binding properties of such compounds play a vital role in their anticancer activity [5, 6]. In the search for effective metal-based drugs, ferrocene and its derivatives were examined and an experimental drug that is a

*Corresponding author. Email: aminbadshah@yahoo.com
§These two authors contributed equally.

ISSN 0095-8972 print/ISSN 1029-0389 online © 2012 Taylor & Francis
http://dx.doi.org/10.1080/00958972.2012.664769

ferrocenyl version of tamoxifen has been reported [7]. Ferrocene has accessible electroactivity and its anticancer activity could be related to its redox processes *in vivo* [8]. Hence, ferrocene-based compounds are promising candidates for biological applications due to their stability, spectroscopic activity, and robust electroactivity [9]. Ferrocenes exert their biochemical action *via* interaction with DNA by mixed binding modes [10]. Several anticancer, antimalarial, and antibacterial agents exert their pharmacological action *via* intercalation with DNA [11].

Ferrocenyl amides containing amino acids and peptides have been developed. The introduction of such groups enables binding biological targets to improve biological applications [12]. Kenny *et al*. [13, 14] assayed a series of ferrocenyl amide (peptide) derivatives against different cancer cell lines and suggested that dipeptides are more active than tri- and tetrapeptides. With this in mind we have synthesized amide derivatives of ferrocene and studied their interaction with DNA using UV-Vis spectroscopy, viscometry, and dynamic laser light scattering (LLS).

2. Experimental

2.1. *Materials and methods*

Ferrocene, *p*-nitroaniline, sodium nitrite, acid chlorides such as benzoyl chloride, *o*-toluoyl chloride, phenyl acetyl chloride, and other chemicals were purchased from Aldrich and used as such. Ferrocenyl-aniline was synthesized by the literature method [15]. Solvents such as ethanol, chloroform, toluene, diethyl ether, and petroleum ether were purified before use according to reported protocols. Melting points were measured with a BIO COTE Model SMP10 melting point apparatus and reported without correction. FT-IR and NMR spectra were obtained with Thermo Scientific Nicolet-6700 FTIR and BRUKER AVANCE 300 MHz NMR spectrometers.

Sodium salt of DNA (Acros) was used as received. Solutions of DNA in 10 mmol L^{-1} phosphate buffer (pH 7.0) gave a ratio of UV absorbance at 260 and 280 nm, A_{260}/A_{280}, of 1.8–1.9, indicating the purity of DNA. Concentrated stock solution of DNA was prepared in 10 mmol L^{-1} phosphate buffer (pH 7.0). The concentration of DNA was determined by UV absorbance at 260 nm after 1 : 100 dilutions. The molar absorption coefficient has been taken as 6600 $(\text{mol L}^{-1})^{-1}\,\text{cm}^{-1}$. Stock solutions were stored below 4°C and used within 4 days.

2.2. *Synthesis of N-(4-ferrocenylphenyl)benzamide (1)*

Solution of benzoyl chloride (0.116 mL, 1.00 mmol) in 10 mL anhydrous toluene was added to the solution of ferrocenyl aniline (0.277 g, 1.00 mmol) and triethylamine (0.68 mL, 1 mmol) in 20 mL anhydrous toluene at 0°C and stirred overnight. The extent of reaction was monitored with thin-layer chromatography. After reaction completion, reaction mixture was filtered and the filtrate was rotary evaporated to get solid product that was recrystallized from chloroform : *n*-hexane (70 : 30) [16]. Yield 75%, m.p. (172–175°C), Anal. Calcd for $C_{23}H_{19}FeNO$ (%): C, 72.46; H, 5.02; N, 3.67. Found: C, 72.40; H, 5.16; N, 3.71. FTIR ($\nu\,\text{cm}^{-1}$) Fe–Cp (478 cm^{-1}), NH (3308 cm^{-1}), CO (1650 cm^{-1}), C=C Ar (1413–1589 cm^{-1}), sp^2 CH (3088.2 cm^{-1}). ^{1}H NMR ($CDCl_3$): 7.89(d, 2 H,

C_6H_5), 7.85(s, 1 H, NH), 7.51(m, 7 H, C_6H_5, C6H4), 4.66(t, 2 H, C_5H_4), 4.33(t, 2 H, C_5H_4), 4.06(s, 5 H, C_5H_5). ^{13}C NMR (75 MHz, $CDCl_3$) (ppm): δ 165.67, 135.78, 135.65, 135.03, 131.90, 128.87, 127.02, 126.63, 120.18, 84.91, 69.63, 68.94, 66.31.

2.3. *Synthesis of N-(4-ferrocenylphenyl)-2-phenylacetamide (2)*

Compound **2** was synthesized by the same method as **1** using phenyl acetyl chloride (0.132 mL, 1 mmol) in place of benzoyl chloride. Yield 80%, m.p. (180–183°C). Anal. Calcd for $C_{24}H_{21}FeNO$ (%): C, 72.93; H, 5.35; N, 3.54. Found: C, 72.89; H, 5.41; N, 3.55. FTIR (ν cm^{-1}) Fe–Cp (477–593 cm^{-1}), NH (3284.9 cm^{-1}), CO (1657 cm^{-1}), C=C Ar(1416–1598 cm^{-1}), sp^2 CH (3058 cm^{-1}). ^{1}H NMR ($CDCl_3$): 7.40(m, 4H, C_6H_4), 7.40(m, 5H, C_6H_5), 7.20(s, 1H, NH), 4.60(t, 2H, C_5H_4), 4.30(t, 2H, C_5H_4), 4.02(s, 5H, C_5H_5), 3.76(s, 2H, CH_2). ^{13}C NMR (75 MHz, $CDCl_3$) (ppm): δ 169.07, 135.52, 135.49, 134.47, 129.58, 129.28, 127.71, 126.44, 119.90, 84.89, 69.57, 68.87, 66.26, 44.85.

2.4. *Synthesis of N-(4-ferrocenylphenyl)-2-methylbenzamide (3)*

Compound **3** was synthesized by the same method as **1** using *o*-toluoyl chloride (0.130 mL, 1.00 mmol) in place of benzoyl chloride. The solid product was recrystallized from chloroform: *n*-hexane (70:30). Yield 83%, m.p. (220°C). Anal. Calcd for $C_{24}H_{21}FeNO$ (%): C, 72.93; H, 5.35; N, 3.54. Found: C, 72.95; H, 5.51; N, 3.49. FTIR (ν cm^{-1}) Fe–Cp (481–495.9 cm^{-1}) NH (3163 cm^{-1}), CO (1642 cm^{-1}), C=C (1415–1594 cm^{-1}), sp^2 CH (3091 cm^{-1}), sp^3 CH (3034 cm^{-1}). ^{1}H NMR ($CDCl_3$): 7.51(m, 6H, C_6H_4, C_6H_4, NH), 7.39(m, 1H, C_6H_4), 7.29(m, 2H, C_6H_4), 4.65(t, 2H, C_5H_4), 4.33(t, 2H, C_5H_4), 4.07(s, 5H, C_5H_5), 2.50(s, 3H, CH_3). ^{13}C NMR (75 MHz, $CDCl_3$) (ppm): δ 167.96, 136.52, 136.47, 135.87, 135.63, 131.33, 130.34, 126.64, 125.96, 119.86, 84.96, 69.62, 68.92, 66.31, 19.92.

2.5. *X-ray crystallography*

For **3**, X-ray data were collected on a Bruker kappa APEXII CCD diffractometer using graphite-monochromated Mo-Kα radiation ($\lambda = 0.71073$ Å). Data collection used ω scans and a multi-scan absorption correction was applied. The structure was solved using SHELXS-97. The hydrogen atoms were generated by geometrical considerations; methyl groups were defined as rigid groups which were allowed to rotate freely. Final refinement on F^2 was carried out by full-matrix least-squares techniques using SHELXL-97. The disordered cyclopentadienyl was refined in two groups as regular pentagons of 1.39 and 1.44 Å. The anisotropic temperature factors of the disordered carbons were restrained to be nearly isotropic.

2.6. *UV-Vis spectrometry*

Absorption spectra were measured on a UV-Visible spectrometer, Shimadzu 1800, at 25 ± 1°C. The electronic spectrum of a known concentration of complex was obtained without DNA. The spectroscopic response of the same amount of complex was then monitored by addition of small aliquots of DNA solution. The DNA-binding constants

of the compounds were calculated by UV-Vis spectroscopy using equation (1). Intercept to slope ratio of the plot 1/[DNA] *versus* $A_o/A - A_o$ gives the value of binding constant K [17].

$$A_o/(A - A_o) = \varepsilon_G/(\varepsilon_{H-G} - \varepsilon_G) + \varepsilon_G/(\varepsilon_{H-G} - \varepsilon_G) \cdot 1/K[\text{DNA}]. \quad (1)$$

2.7. *Viscosity measurements*

Viscosity experiments were carried out on an Ubbelodhe viscometer, immersed in a thermostated water-bath maintained at 25 ± 0.5°C. The concentration of DNA was 200 μmol L^{-1}. Data were presented as $[\eta/\eta_o]^{1/3}$ *versus* $R = [\text{comp}]/[\text{DNA}]$, where η/η_o is the viscosity of DNA in the presence of complex and η_o is the viscosity of DNA alone. Viscosity (η) values were calculated from the observed flow time of DNA-containing solution ($t > 100$ s) corrected for the flow time of buffer alone (t_o), $\eta = (t - t_o)/t_o$ [18].

2.8. *LLS measurements*

Dynamic LLS experiments were carried out with a Brookhaven BI 200 S instrument fitted with He–Ne laser (wavelength, $\lambda = 638$ nm) and a BI 9000 AT digital correlator; details of the LLS instrumentation and theory can be found elsewhere [19, 20].

Correlation functions from dynamic light scattering were analyzed by the constrained regularized CONTIN method [21]. Distributions of decay rate, Γ, were converted to distributions of apparent mutual diffusion coefficient,

$$D_{app} = \Gamma/q^2, \quad (2)$$

where $q = (4\pi n/\lambda)\sin(\theta/2)$, n is the refractive index of the solvent, and θ is the scattering angle. Hence, distributions of apparent hydrodynamic radius were evaluated using the Stokes–Einstein relationship,

$$r_{h,\,app} = kT/(6\pi\eta D_{app}), \quad (3)$$

where k is the Boltzmann constant, T is the absolute temperature, and η is the viscosity of the solvent. LLS measurements were taken at constant temperature of 25°C. A series of solutions were made with constant concentration of DNA and varying concentration of complex. All of the samples were filtered with 0.45 μm filters in order to remove dust completely.

3. Results and discussion

3.1. *Synthesis and spectroscopic studies*

Ferrocenyl amides have been synthesized by reacting ferrocenyl aniline with different acid chlorides under N_2 using anhydrous toluene as solvent (scheme 1). All the synthesized compounds were characterized by several analytical techniques.

FT-IR spectra of **1**–**3** displayed a broad peak for N–H bond at 3344–3402 cm^{-1} due to hydrogen-bonding. The hydrogen-bonding was confirmed by the crystal structures of

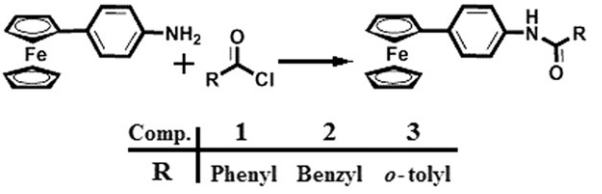

Scheme 1. Synthesis of ferrocenyl amides.

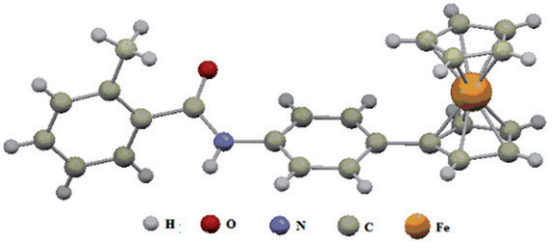

Figure 1. Molecular structure of **3**.

1 and **3**. The diagnostic peak in the range 1610–1730 cm^{-1} was assigned to carbonyl; aliphatic and aromatic protons appeared in the normal ranges. ^{1}H NMR and ^{13}C NMR signals for all amides appeared in the expected regions (section 2).

UV-Vis spectra of these amides were taken in 80% ethanol. The appearance of peaks at 440–450 nm corresponds to d–d electronic transitions. In UV-region, two peaks at 256 and 292 nm for **2** may be attributed to π–π^* transition of benzene ring and π–π^* transition in the Cp rings of ferrocene, respectively. In **1** and **3,** both UV-region peaks merged into a single broad peak with maximum absorbance at 296 nm (**1**) and 292 nm (**3**).

3.1.1. X-ray structure of 3. Orange crystals of **1** and **3** were obtained by slow evaporation from toluene. The X-ray structure of **1** has already been reported by our research group [16]; the structure of **3** is shown in figure 1. The crystal of **3** is monoclinic, **s**pace group is $P\,21/c$, correction method used multi-scan; $a = 8.6329(3)$ Å, $b = 20.6226(9)$ Å, $c = 22.7784(9)$ Å, $\beta = 96.215\ (1)^\circ$, $\mu = 0.760\ mm^{-1}$, $V = 4031.5(3)$ $Å^3$, $Z = 8$, $D_x = 1.303\ g\,cm^{-3}$, $F(000) = 1648.0$, $T = 296$ K, $1.98^\circ \le \theta \le 28.32^\circ$, $(h,\ k,\ l)_{max} = (11,\ 27,\ 30)$ and the final R factor $R_1 = 0.0505$, $wR_2 = 0.1423$. The selected bond lengths and angles are given in table 1.

In **3** the cyclopentadienyl ring A (C6–C10), phenyl rings B (C11–C16), and C (C18–C23) are planar with r.m.s. deviations of 0.0024, 0.0020, and 0.0030 Å, respectively. The dihedral angle between A/B is 8.72(4)°, which shows that central phenyl is almost planar with attached cyclopentadienyl. The dihedral angle between B/C is 94.24°. The unsubstituted cyclopentadienyl ring of ferrocene is disordered over two sites with occupancy ratio of 0.548 (14) : 0.452 (14), figure 1. The packing diagram of **3** (figure 2) shows a supramolecular chain structure mediated by NH–O and π–H secondary non-covalent interactions. In this chain molecules are helices due to screw symmetry.

Table 1. Selected bond lengths (Å) and angles (°) of **3**.

N–H	0.859(2)	C6–Fe1–C7	40.81(15)
C17–O	1.227(5)	C6–Fe1–C8	68.11(17)
C17–N	1.341(3)	C6–Fe1–C9	68.32(16)
C14–N	1.423(7)	C6–Fe1–C10	40.66(14)
Fe1–C6	2.034(3)	C7–Fe1–C8	40.32(18)
Fe1–C7	2.030(4)	C7–Fe1–C9	68.47(17)
Fe1–C8	2.028(4)	C7–Fe1–C10	68.72(15)
Fe1–C9	2.039(4)	C8–Fe1–C9	40.79(16)
Fe1–C10	2.059(3)	C8–Fe1–C10	68.55(15)
		C9–Fe1–C10	40.80(14)
		C1–Fe1–C9	122.2(3)

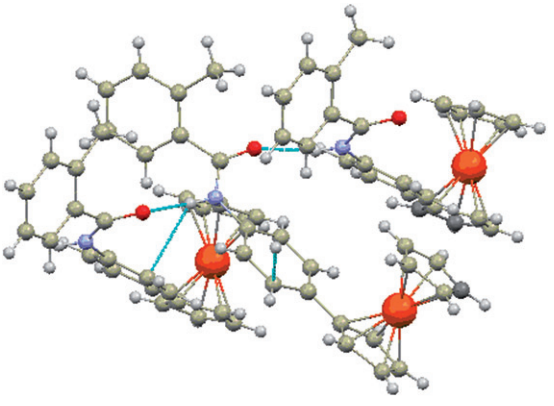

Figure 2. Supramolecular structures of **3** mediated by NH–O (2.009 Å) and π–H (2.777–2.684 Å).

The capability of complex to form secondary interactions is a prerequisite for DNA-binding ability.

3.2. *DNA-binding studies*

Binding of small molecules to DNA can be detected by a number of techniques. Here we report DNA-binding studies of new ferrocenyl amides using UV-Vis absorption, viscometry, and dynamic LLS.

3.2.1. UV-Vis spectroscopy. UV-Vis spectroscopy is employed for study of ferrocenes owing to their intense color. The color of the ferrocenes strongly changes upon oxidation, thus allowing spectroscopic measurements in the visible range. UV-Vis spectroscopy is an effective tool for quantification of binding strength of DNA with metal complexes. The DNA-binding constants (K_b) of **1**–**3** (table 2) were calculated from UV-Vis spectroscopic data by using equation (1).

Compound **1** showed maximum absorbance at 296 nm. Upon addition of various concentrations of DNA a steady decrease in absorbance accompanied with red shift of 10 nm was observed (figure 3). The red shift is indicative of partial intercalation with the

Table 2. The binding constants and Gibbs free energies of **1**–DNA, **2**–DNA, and **3**–DNA complexes as determined by UV-V is spectroscopy.

Compound DNA complex	[a]ε_o ((mol L^{-1})$^{-1}$ cm^{-1})	K_b ((mol L^{-1})$^{-1}$)	$-\Delta G$ (kJ mol^{-1})
1–DNA	–	9.8×10^3	22.770
2–DNA	2.08×10^3	6.3×10^3	21.675
3–DNA	2.74×10^3	4.3×10^3	20.729

[a]ε_o is the molar absorptivity coefficient.

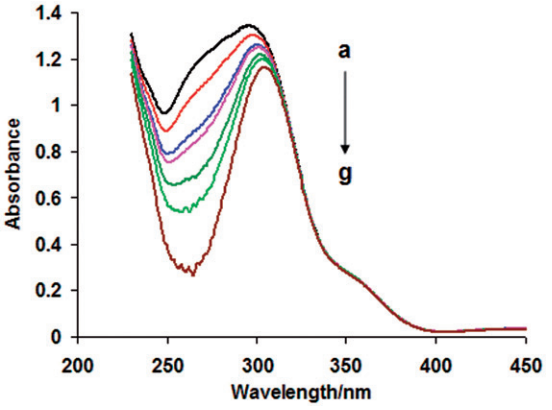

Figure 3. UV-V is spectroscopic response of 0.5 mmol L^{-1} *N*-(*p*-ferrocenylphenyl) benzamide (**1**) in the absence (a) and presence of 20(b), 40(c), 62(d), 83(e), 104(f), and 125(g) μmol L^{-1} DNA.

π^* orbital of the intercalating ligand coupling with the non-bonding orbital of the base pairs, decreasing the π–π^* transition energy, and resulting in bathochromism. Partial filling of the coupling π orbital by electrons is expected to decrease the transition probabilities, resulting in hypochromism. Compound **3** also exhibited similar behavior, but with smaller binding constant. These complexes show partial intercalation due to planarity in the molecule, as shown by single-crystal X-ray analysis. Compound **3** has smaller binding constant due to the presence of *o*-methyl which decreases the planarity of the complex. Recently Qureshi *et al*. [22] investigated the mechanism of action and binding constant of protonated ferrocene. Our results show that ferrocenyl amides are better intercalators than protonated ferrocene. This may be due to the presence of amide in the structure that could interact with DNA bases *via* hydrogen-bonding, as previously reported for benzamide [23].

UV spectra of **2** have two peaks in the UV region. One at 257 nm is attributed to the π–π^* transition in Cp ring of ferrocene and the other at 291 nm, from π–π^* transition of electrons in the benzene ring. The UV-Vis spectral response of **2** on gradual addition of DNA (figure 4) showed decrease in absorption maximum with slight blue shift. The hypochromism and hypsochromic shift indicate penetration of benzyl group capable of forming π–H-bonding (π-stacking) with DNA bases. At the same time the part of the compound that absorbs at 250 nm shows DNA damage, obvious from hyperchromism in that region. The isosbestic point can be due to equal increase of DNA fragments by the probable DNA damage with increasing concentration of compound-DNA complex.

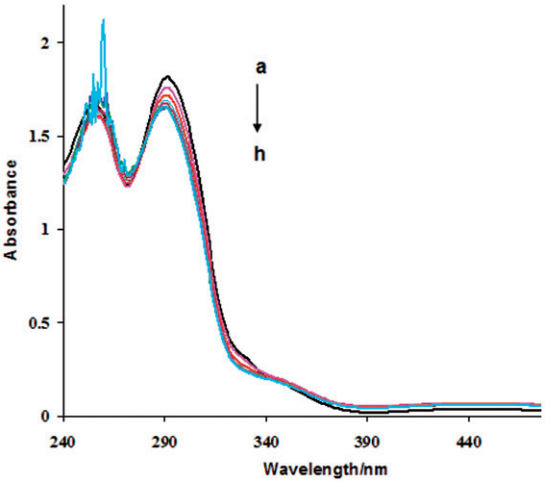

Figure 4. UV-V is spectroscopic response of 0.5 mmol L^{-1} *N*-(*p*-ferrocenylphenyl)phenyl acetamide (**2**) in the absence (a) and presence of 20(b), 40(c), 62(d), 83(e), 104(f), 125(g), and 146(h) μmol L^{-1} DNA.

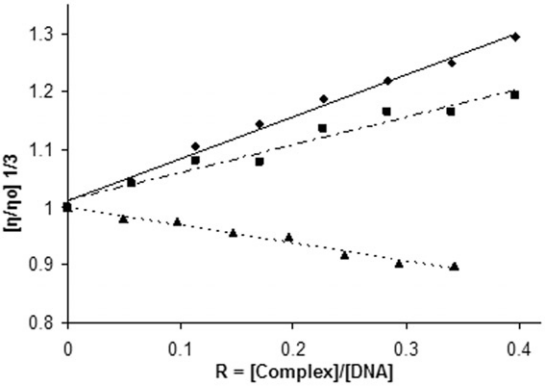

Figure 5. Variation of relative viscosity $[\eta/\eta_o]^{1/3}$ of 200 μmol L^{-1} DNA with increasing concentration of **1** (--◆--), **2**(--▲--), and **3** (--■--).

3.2.2. Viscometry. Viscometric technique is an effective tool to clarify the mode of interaction of small molecules with DNA. In general, intercalation causes an increase in viscosity of DNA solution due to lengthening of the DNA helix as the base pair pockets are widened to accommodate the binding molecule [24]. The effect of increasing concentration of **1** and **3** on the viscosity of DNA is shown in figure 5. The relative viscosity of DNA increases with increase in concentration of **1** and **3**, a behavior which is similar to DNA-binding agents with intercalation as the dominant mode [25–27]. The viscosity results clearly show that intercalation is the prevailing mode of interaction of **1** and **3** with DNA. The greater slope of the plot shows that **1** intercalates more deeply than **3**. As evident from the crystal structure, **1** is more planar (with dihedral angle 69.67° between B and C ring) than **3** (94.24°).

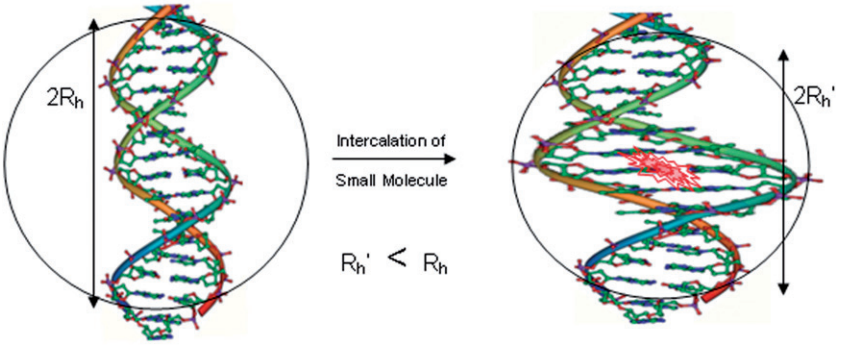

Figure 6. Decrease in the hydrodynamic radius (R_h) upon intercalation of complex in the DNA helix.

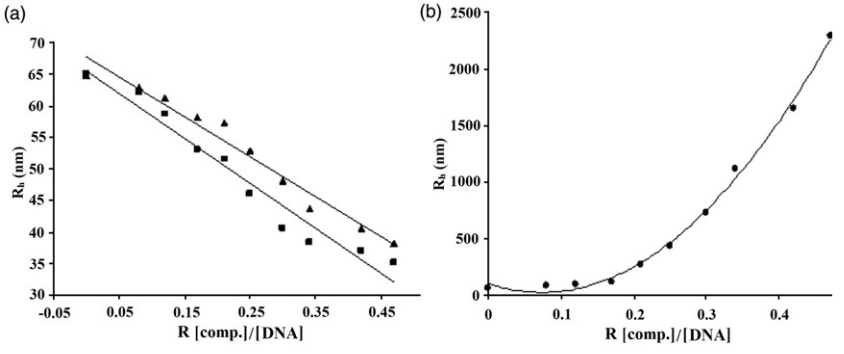

Figure 7. Variation of hydrodynamic radius (R_h) of 200 μmol L^{-1} DNA with increasing concentration of (a) **1** (--▲--) and **3** (--■--), (b) **2**.

In contrast, electrostatic interactions cause compactness and aggregation of DNA. The aggregation reduces the number of independently moving DNA molecules which results in lowering of the solution viscosity [17]. The plot of relative viscosity $[\eta/\eta_o]^{1/3}$ *versus r* (r = [complex]/[DNA]) is shown in figure 5. The plot reveals negative change in relative viscosity with increasing concentration of **2**. These results suggest electrostatic or groove binding of **2** with DNA, which corresponds to the flexibility of its structure due to the presence of benzyl.

3.2.3. Dynamic LLS studies. Upon intercalation of a small molecule into the DNA-helix, the expansion of the DNA helix occurs, i.e., cavities are created to accommodate small molecules between the bases, reducing hydrodynamic radius (R_h) as shown in figure 6.

Figure 7 shows the change in R_h with increasing concentration of **1**, **2**, and **3** at constant concentration of DNA. Plot of R_h *versus R* {[complex]/[DNA]} of **1** and **3** shows that R_h decreases with increasing concentration of complexes, indicating the

dominance of intercalation of **1** and **3** into DNA. The more negative slope of **1** can be attributed to deeper intercalation into DNA than **3**.

On the other hand, groove binding or electrostatic interaction of small molecule with DNA causes compactness or aggregation of DNA, which in fact increases the size of DNA and subsequently increases the R_h of DNA. The increased R_h of DNA with increasing concentration of **2** is a clear indication of the electrostatic interaction of **2** with DNA.

4. Conclusions

The ability of new ferrocenyl amides to form intermolecular hydrogen-bonding (see packing diagram) was exploited to conclude that partial intercalation of these compounds with DNA may be due to formation of similar kind of hydrogen bonds with DNA bases. The results suggest that the anticancer properties of metallo-drugs can be improved by incorporation of such substituents in the structure having the potential to establish strong non-covalent secondary interactions with DNA-bases. This study provides a further step in designing anticancer metal-based drugs.

Supplementary material

CCDC 815185 contains the supplementary crystallographic data for **3**. These data can be obtained free of charge *via* http://www.ccdc.cam.ac.uk/conts/retrieving.html (or from the Cambridge Crystallographic Data Centre, 12 Union Road, Cambridge CB2 1EZ, UK; Fax: +44 1223 336033).

Acknowledgments

We are grateful to Higher Education Commission and Quaid-i-Azam University, Islamabad, Pakistan for financial support.

References

[1] S.S. Hall. *New York Times Mag*., **147**, 64 (1997).
[2] T.R. Krugh. *Curr. Opin. Struct. Biol*., **4**, 351 (1994).
[3] S. Neidle. *Biopolymers*, **44**, 105 (1997).
[4] B.H. Geierstanger, D.E. Wemmer. *Annu. Rev. Biophys. Biomol. Struct*., **24**, 463 (1995).
[5] K. Akdi, R.A. Vilaplana, S. Kamah, F.G. Vilchez. *J. Inorg. Biochem*., **99**, 1360 (2005).
[6] K.E. Erkkila, D.T. Odom, J.K. Barton. *Chem. Rev*., **99**, 2777 (1999).
[7] The Language of Biochemistry. Available online at: http://www.medscape.com/medline/abstract/14613131 (accessed 18 February 2012).
[8] D. Osella, M. Ferrali, P. Zanello, F. Laschi, M. Fontani, C. Nervi, G. Cavigiolio. *Inorg. Chim. Acta*, **306**, 42 (2000).
[9] B. Lal, A. Badshah, A.A. Altaf, N. Khan, S. Ullah. *Appl. Organomet. Chem*., **25**, 843 (2011).

[10] S. Sato, T. Nojima, M. Waki, S. Takenaka. *Molecules*, **10**, 693 (2005).
[11] S. Neidle. *Prog. Med. Chem.*, **16**, 151 (1979).
[12] Á. Mooney, A.J. Corry, D. O'Sullivan, D.K. Rai, P.T.M. Kenny. *J. Organomet. Chem.*, **694**, 886 (2009).
[13] A. Goel, D. Savage, S.R. Alley, T. Hogan, P.N. Kelly, S.M. Draper, C.M. Fitchett, P.T.M. Kenny. *J. Organomet. Chem.*, **691**, 4686 (2006).
[14] A.J. Corry, N. O'Donovan, Á. Mooney, D. O'Sullivan, D.K. Rai, P.T.M. Kenny. *J. Organomet. Chem.*, **694**, 880 (2009).
[15] A.A. Altaf, N. Khan, A. Badshah, B. Lal, Shafiqullah, S. Anwar, M. Subhan. *J. Chem. Soc. Pak.*, **33**, 691 (2011).
[16] A.A. Altaf, A. Badshah, N. Khan, M.N. Tahir. *Acta Cryst.*, **E66**, m831 (2010).
[17] A. Shah, M. Zaheer, R. Qureshi, Z. Akhter, M.F. Nazar. *Spectrochim. Acta, Part A*, **75**, 1082 (2010).
[18] S. Satyanarayana, J.C. Dabrowiak, J.B. Chaires. *Biochemistry*, **32**, 2573 (1993).
[19] R. Pecora, J. Berne. *Dynamic Light Scattering*, Plenum Press, New York (1976).
[20] B. Chu. *Laser Light Scattering*, 2nd Edn, Academic Press, New York (1991).
[21] S.W. Provencher. *Comput. Phys. Commun.*, **27**, 213 (1982).
[22] A. Shah, R. Qureshi, N.K. Janjua, S. Haque, S. Ahmad. *Anal. Sci.*, **24**, 1437 (2008).
[23] J. Mclick, A. Hakam, P.I. Bauer, E. Kun, D.E. Zacharias, J.P. Glusker. *Biochim. Biophys. Acta*, **909**, 71 (1987).
[24] J.M. Veal, R.L. Rill. *Biochemistry*, **30**, 1132 (1991).
[25] M. Cory, D.D. Mckee, J. Kagan, D.W. Henry, J. Miller. *J. Am. Chem. Soc.*, **107**, 2528 (1985).
[26] M.J. Waring. *J. Mol. Biol.*, **13**, 269 (1965).
[27] C. Hiort, P. Lincoln, B. Norden. *J. Am. Chem. Soc.*, **115**, 3448 (1993).